Published in final edited form as:
Nat Cell Biol. 2014 January ; 16(1): 87–98. doi:10.1038/ncb2887.

Calcium dependent regulation of Rab activation and vesicle fusion by an intracellular P2X ion channel

Katie Parkinson[1], **Abigail E. Baines**[1], **Thomas Keller**[1], **Nicole Gruenheit**[1], **Laricia Bragg**[2], **R. Alan North**[1,2], and **Christopher R.L. Thompson**[1,*]

[1]Faculty of Life Sciences, University of Manchester, Michael Smith Building, Oxford Road, Manchester M13 9PT, United Kingdom

[2]Faculty of Medical and Human Sciences, University of Manchester, Michael Smith Building, Oxford Road, Manchester M13 9PT, United Kingdom

Abstract

Rab GTPases play key roles in the delivery, docking and fusion of intracellular vesicles. However, the mechanism by which spatial and temporal regulation of Rab GTPase activity is controlled is poorly understood. Here we describe a mechanism by which localized calcium release through a vesicular ion channel controls Rab GTPase activity. We show that activation of P2XA, an intracellular ion channel localized to the *Dictyostelium discoideum* contractile vacuole system, results in calcium efflux required for downregulation of Rab11a activity and efficient vacuole fusion. Vacuole fusion and Rab11a downregulation require the activity of CnrF, an EF hand containing Rab GAP found in a complex with Rab11a and P2XA. CnrF Rab GAP activity to Rab11a is enhanced by the presence of calcium and the EF-hand domain. These findings suggest that P2XA activation results in vacuolar calcium release, which triggers activation of CnrF Rab GAP activity and subsequent downregulation of Rab11a to allow vacuole fusion.

Introduction

Regulation of intracellular vesicle traffic is fundamental for normal cell function and its mis-regulation is associated with congenital developmental disorders, cancer and neurological dysfunction [1]. Studies of vesicle traffic in different systems have revealed the evolutionarily conserved role played by Rab GTPases. Every organelle of both the endocytic and exocytic pathways expresses several Rab GTPases, which must be sequentially activated to allow precise delivery, docking and fusion of different membrane compartments [2-6]. Another regulator of vesicle fusion events is intracellular calcium. Transient and localized increases in calcium have been shown to facilitate some, but not all, vesicle fusion events [7-19]. However, it is currently unknown whether interplay between calcium and Rab GTPases, could coordinately regulate vesicle fusion.

The *Dictyostelium discoideum* contractile vacuole (CV) system is an intracellular vesicle required for osmoregulation. The CV cycle is a highly regulated process, orchestrated by

[*]Correspondence should be addressed to CRLT (christopher.thompson@manchester.ac.uk) .

Contributions K.P. performed most of the experiments. A.E.B. performed the electrophysiology, P2XA point mutant and GCaMP2 studies; T.K. created the CnrF RabGAP knockout strain; N.G. performed the bioinformatic analysis of EF hand containing RabGAPs; L.B. created the P2XA point mutants for expression in HEK cells. C.R.L.T. and R.A.N. conceived of the study and wrote the manuscript. All authors discussed the results, and contributed to writing or commenting on the manuscript.

Competing Financial Interests: The authors declare no competing financial interests

Europe PMC Funders Author Manuscripts

Rab proteins, their regulators and their effectors [20-27]. The contractile vacuole is also an acidic calcium store (acidocalcisome) [28], and therefore provides an excellent model system to study the coordinated regulation of vesicle trafficking by Rab proteins and calcium. Upon hypo-osmotic shock, water enters tubules of the CV system, a process accompanied by activation of Rab11a which is localized to CV membranes [22, 25]. Drainin, a putative volume-sensing Rab11a-GTP binding protein, is subsequently recruited to maturing vacuoles [20, 22, 29, 30]. Next, vacuoles are prepared for fusion with the plasma membrane through the recruitment of the Rab GAP, Disgorgin, and Rab8a [22, 23]. Once tethered to the plasma membrane, the 'non-polarised' CV becomes 'polarised' and committed to pore formation [23]. This process is defined by a 'ring to patch transition', in which different proteins become concentrated at the front or back of the CV [23]. How the correct spatial and temporal regulation of these Rab proteins is achieved is poorly understood.

Recently, we discovered that a homologue of mammalian P2X receptors, P2XA, is exclusively localized to the *Dictyostelium* CV system [31]. P2X receptors are calcium-permeable ion channels gated by ATP which function in diverse physiological processes [32, 33]. However, the intracellular localization of P2XA in *Dictyostelium* cells is inconsistent with a role in regulating responses to extracellular ATP[31]. Instead, P2XA knockout cells exhibit defects in responses to hypo-osmotic shock[31, 34] (Supplementary Figure 1). Under hypo-osmotic shock, knockout cells become rounded and the rate of CV discharge is much reduced[31, 34]. This raises the possibility that P2XA may be an important conduit for vacuolar calcium release, and that this calcium is required for the correct regulation of vacuolar cycling [35]. However, major questions remain unanswered. Firstly, it is unknown whether the intracellular function of P2XA indeed requires ion channel activity and calcium flux. Secondly, it is unknown whether disruption of P2XA activity, and therefore calcium flux, affects vesicle fusion or some other event in the CV cycle, such as maturation or delivery. Finally, it is unknown how an ATP-gated ion channel could regulate a Rab-GTP dependent process in a calcium-dependent manner at the molecular level.

Results

Intracellular P2XA function requires ion channel activity

To determine if P2XA ion channel activity is required for osmoregulation, mutations were generated that resulted in inactive (K67A/K289A), less active (R285K), or hyperactive (R63A) versions of P2XA when tested in HEK293 cells (Figure 1A and B). Next, gene replacement *Dictyostelium* strains were generated in which the endogenous gene was replaced with wild-type or point mutated versions and tested for osmotic shock defects. In each case mutated receptors still localized to the contractile vacuole (Supplementary figure 2). However, the gene replacement strains exhibited clear differences in their ability to respond to osmotic shock, with responsiveness correlating very well with ion channel activity (Figure 1 C and D).

P2XA mutant cells exhibit aberrant contractile vacuole system morphology

Previous studies have suggested that P2XA disruption results in a prolonged CV cycle with fewer fusion events [31]. We next sought to determine whether these defects were due to a failure in CV maturation, trafficking, tethering, pore formation or fusion. To address this, we firstly examined the morphology and dynamics of the CV system following hypo-osmotic shock in cells expressing Dajumin-GFP, which labels the CV system throughout the cycle. These studies showed that the CV system was strikingly aberrant in P2XA mutant cells (Figure 2A and Supplementary Videos 1 and 2). Mutant cells contained many more vacuoles (Figure 2B), which were not only found at the bottom of the cell where it contacts the substratum, but unlike in wild-type cells, also throughout the cell (Figure 2C). Although

many of these vacuoles appeared to be statically tethered to the plasma membrane, few fusion events were observed (Figure 2D and E). Finally, the P2XA mutant vacuoles were typically smaller than wild-type vacuoles (Figure 2F). Live cell imaging revealed this was not due to a simple failure to mature to the correct size. Instead normal-sized vacuoles did form but tended to split into multiple smaller vacuoles after prolonged periods of tethering (Figure 2G).

P2XA is required for vacuoles to transition from tethered to fused states

As the P2XA mutant contains large numbers of vacuoles which are tethered but do not fuse, we next tested whether this might be explained by a failure to recruit, or correctly localize, factors required for vesicle maturation or fusion. Firstly, we found that Drainin (a marker for vesicle maturation and tethering) localized to all mutant vesicles even when very small (Figure 3A and Supplementary Videos 3 and 4). Secondly, Rab8-GFP, a marker normally only transiently recruited to mature vesicles just prior to fusion, localized to most mutant vesicles (Figure 3B and Supplementary Videos 5 and 6). In wild-type cells, tethered vesicles expressing Drainin and Rab8 quickly undergo a dynamic rearrangement (‘ring to patch’ transition), which is required for recruitment of the pore formation complex and thus efficient fusion. Most notably, in wild-type cells, seconds after Rab8 was recruited to the vacuole, Drainin disappeared from the site of contact with the plasma membrane, followed by a reciprocal enrichment of Rab8 at the point of plasma membrane contact. In contrast, in P2XA mutant cells, this ‘ring to patch’ rearrangement of Drainin and Rab8 did not occur, thus providing an explanation for inefficient fusion (Figure 3A and B). From these observations, many P2XA mutant vacuoles therefore appear to be ‘trapped’ in a mature, membrane-tethered and fusion-competent state, yet are unable to undergo fusion.

P2XA activity is dynamically regulated during the CV cycle

The above genetic studies suggest that P2XA receptors function to promote vacuole fusion. Since P2XA is present throughout the entire CV cycle (Supplementary figure 4), we next tested whether the temporal regulation of P2XA activity was consistent with its apparent function. For this, we developed a sensor for P2XA ion channel activity in which the calcium-sensitive GCaMP2 reporter is fused to the C-terminus of the P2XA receptor. Because P2XA encodes a calcium-permeable ion channel, we reasoned that channel activation would result in a transient fluorescence increase. Indeed, an analogous FRET based system has been successfully employed to monitor mammalian neuronal P2X receptor activation [36]. We found that when P2XA-GCaMP2 was expressed in HEK293 cells, the presence of the GCaMP2 tag did not affect the concentration response curves to ATP (Figure 4A and B). Furthermore, P2XA-GCaMP2 acted as a reporter for P2XA activity, because when changes in fluorescence were used to measure dose responses, measurements were similar to those achieved with electrophysiological recordings, and detectable at concentrations as low as 30μM ATP (Figure 4C and Supplementary Figure 4). Fluorescence imaging also revealed these transient increases upon stimulation with ATP fluorescence initially took place at the plasma membrane (Figure 4D, Supplementary Figure 4 and Supplementary Videos 7 and 8). Finally, fluorescence increases were dependent on ion channel activity as P2XA(K67A/K289A)-GCaMP2 showed no change upon ATP stimulation (Figure 4E and Supplementary Figure 4).

We next tested whether the P2XA-GCaMP2 fusion protein was fully functional in *Dictyostelium* cells. P2XA-GCaMP2 was found to specifically localize to the CV system (Figure 4G and Supplementary Video 9) and overexpression effectively rescued the P2XA null osmoregulation defects (Supplementary Figure 5). Furthermore, in control experiments, GCaMP2 alone acted as an efficient calcium sensor in *Dictyostelium* cells (Supplementary Figure 5). Based on these findings, we used CV P2XA-GCaMP2 fluorescence to measure

channel activity *in vivo*. P2XAGCaMP2 fluorescence was measured at different CV stages: early, docked and during fusion. We found that fluorescence, and thus P2XA activity, was highest when contractile vacuoles were docked or underwent fusion (Figure 4F and G and Supplementary Videos 9 and 10). These changes in fluorescence were dependent on P2XA ion channel activity, since the inactive P2XA(K67A/K289A)-GCaMP2 mutant showed no increase in fluorescence (Figure 4F and G and Supplementary Video 11). This also correlated with a failure of this strain to undergo the 'ring to patch' transition (Figure 4G and Supplementary Video 11). These findings provide further support for the idea that increases in calcium levels are required for CV fusion. Finally, they suggest that the changes in calcium levels that result in increased GCaMP2 fluorescence are due to calcium efflux from the vacuole via the P2X ion channel, rather than coincident increases in calcium levels in or around the contractile vacuole at this stage.

P2XA is required to inhibit Rab11 activity

To gain insight into how P2XA activation affects CV fusion at the molecular level, we took a proteomic approach to identify candidate proteins regulated by P2XA. For this, tagged versions of P2XA were expressed in *Dictyostelium* cells and used to pull down interacting proteins, which were identified by mass spectrometry (Figure 5A and Supplementary Table 1). One major interacting protein was Rab11a (Figure 5B). Consistent with previous studies [25], Rab11a-RFP was localized to the CV system where it co-localised extensively with P2XA (Figure 5C). Moreover, we found that clones that expressed high levels of Rab11a exhibited CV system defects similar to those observed when P2XA function was disrupted, with large numbers of small vacuoles adjacent to the plasma membrane (Figure 5D). Furthermore these clones showed severe defects in osmotic shock responses (Figure 5D). Importantly, it is likely that these defects are due to changes in the level of Rab11 activation, because pull downs on cell extracts with an antibody that is highly specific for activated Rab11a-GTP (Supplementary Figure 6) revealed that even though the ratio of active Rab11a-GTP: inactive Rab11a-GDP was the same in each clone, the absolute levels of activated Rab11a-GTP correlated well with the observed defects (Figure 5E). Based on these observations, we reasoned that a simple explanation for the similarity in phenotype between the P2XA mutant and Rab11a overexpressing clones is that P2XA is required to inhibit Rab11a activity. Consistent with this idea, pull down assays using the Rab11a-GTP specific antibody revealed the *ratio* of bound active Rab11a-GTP: unbound inactive Rab11a-GDP was significantly increased in P2XA mutant cells (Figure 5F and G). Consequently, P2XA mutant cells exhibited an almost 2.5 fold increase in the levels Rab11a-GTP, which was comparable to increases in Rab11a overexpression sufficient to generate the same osmoregulation phenotype (Figure 5D-G).

CnrF encodes a calcium regulated Rab GAP required for Rab11 inactivation

Since the P2XA ion channel is calcium-permeable, we reasoned that calcium passing through the activated channel could provide a regulatory mechanism for Rab activity regulation. We thus took a bioinformatic approach to identify putative calcium-sensitive regulators of Rab activity. Rab activity is controlled by the opposing actions of inactivating Rab GAPs and activating Rab GEFs. Whilst Rab GEFs remain poorly characterized, Rab GAPs can be identified by virtue of the conserved TBC domain. These studies resulted in the identification of a conserved family of proteins containing both a putative TBC Rab GAP domain and calcium binding EF hand (Supplementary Figure 7). Since the *Dictyostelium* genome encodes three such proteins, to test whether any were involved in Rab11a regulation, single gene disruption strains were generated. Consistent with this idea, we found that knockout of one such gene, *cnrF*, resulted in osmotic shock and contractile vacuole defects identical to those observed in P2XA null mutant or Rab11a overexpressing cells (Figure 6A, B and C). Furthermore, gene replacement strains in which the wild type

cnrF locus was replaced by versions containing specific point mutations that disrupt either GAP activity (R270A)[37] or calcium binding by the EF hands (E623Q/D659Q)[38] were indistinguishable from the null mutant in their osmoregulation phenotype (Figure 6A, B and C). Finally, disruption of *cnrF* activity, and point mutations that disrupt EF hand function or Rab GAP activity, all led to a significant increase in ratio of active Rab11a-GTP: inactive Rab11a-GDP (Figure 6 D and E). In contrast, *cnrF* overexpression led to a significant decrease in the ratio of Rab11a-GTP: Rab11a-GDP ratio compared to wild type cells (Figure 6 D and E).

The above results suggest that *cnrF* encodes a calcium regulated Rab11a Rab GAP. To further test this idea we next measured the Rab GAP activity of bacterially expressed *cnrF*[22, 37]. Firstly, we found that CnrF exhibited GAP activity towards Rab11a, but not Rab8, another contractile vacuole localized Rab (Figure 7A and B). Secondly, the efficiency of GAP activity was greatly increased by the presence of calcium (Figure 7A-E). Importantly, this calcium dependent increase was dependent on the presence of the EF hand domain (Figure 7A and B). It is noteworthy, however, that deletion of the EF hands did not completely eliminate GAP activity, as activity could be detected when a high concentration of truncated CnrF was added to the *in vitro* assay (Figure 7A and B). Therefore, calcium binding through the EF hand appears to play a crucial role in regulating the efficiency of *cnrF* Rab GAP activity. This idea was further supported by *in vivo* studies, because rescue of the *cnrF* mutant osmoregulation defects required much greater levels of exogenous expression of the EF hand truncated version of *cnrF*, when compared to full length *cnrF* (Figure 8A). Similar findings were observed when the EF hand point mutant was expressed in *cnrF* mutant cells, although rescue was never seen with the Rab GAP domain point mutant, further highlighting the critical importance of Rab GAP activity for *cnrF* function (Figure 8B). Finally, although CnrF was not specifically localized to the contractile vacuole (Figure 8C), both full length and truncated CnrF interacted with P2XA and Rab11a in pull down assays (Figure 8D) in the presence and absence of calcium (Figure 8E). These findings suggest that CnrF exists in a protein-protein complex with Rab11a and P2XA, and that it is the Rab GAP activity, rather than the binding of CnrF to Rab11a, that is regulated by calcium (Figure 8F).

Discussion

Precise regulation of the *Dictyostelium* CV cycle requires the correct spatial and temporal regulation of a Rab small GTPase cascade, as well as the activity of the CV localized P2XA receptor ion channel. We show that activation of P2XA results in localized increases in calcium concentration, which activates a calcium-sensitive Rab GAP and in turn downregulates its target Rab11a which is required for vesicle fusion with the plasma membrane (Figure 8F). Interestingly, earlier studies have revealed that Rab11a localization does not change upon vacuole fusion[22, 23, 25]. However, the Rab11-GTP specific binding protein, Drainin, is removed from the membrane at the fusion site, as predicted by our model[22, 23]. Furthermore, expression of constitutively active Rab11a blocks this redistribution of Drainin[22]. These findings suggest that the rate of Rab11a effector dissociation is faster than the rate of removal of inactivated Rab11-GDP from the CV membrane. It is therefore likely that CV fusion requires a change in Rab11a activity at the site of vacuole fusion, but not redistribution of Rab11a itself, only its effector Drainin. Thus, this study provides a mechanistic link between P2X ion channel activity and Rab regulated vesicular trafficking.

Our data provide further evidence that P2X receptors can play a role in regulating intracellular events, in addition to their well-established role in regulating responses to extracellular ATP. However, it is important to note that P2X receptors are also expressed on

intracellular membranes in some cell types of higher organisms [39, 40]. Furthermore, evidence is emerging to support their functional importance. For example, P2X4 receptors have been shown to localise to exocytic lamellar bodies, intracellular vesicles found within alveolar type II epithelial cells [39]. Expression of dominant negative P2X4 in these cells has led to the suggestion that endogenous P2X4 is required to stabilize and expand the fusion pore to allow sufficient release of lung surfactant [39], although the molecular mechanism has not been determined.

As the function of P2XA receptors in contractile vacuole fusion requires intact ATP binding residues, this begs the question how channel activity is regulated. To date, only ATP has been shown to act as an efficient ligand for P2XA[34]. So, where does the ATP come from and how are its levels controlled? Firstly, it seems likely that the ATP must come from the vacuole itself, rather than the extracellular space, as hypo-osmotic shock and activation of P2XA occurs when the cells are placed in water. Secondly, the putative ATP binding domain of P2XA has been shown to reside within the lumen of the CV [35, 41]. One possibility, therefore, is that ATP, although present throughout the contractile vacuole cycle, acts as a permissive ligand that is only able to activate the receptors when the ionic conditions or pH encountered are optimal. Some support for this idea comes from our recent finding that the ionic and proton environment encountered by the ATP binding domain (i.e. that of the lumen of the vacuole) has a large effect upon the level of P2XA activation [34]. Moreover, the contractile vacuole contains a high concentration of proton pumps (V-type ATPases) [42], and best estimates suggest that the vesicles may be acidified to pH 6.2 [43]. Under these conditions the P2XA channel is rapidly desensitized, and may remain so under conditions of continued acidification [34]. However, when the vacuole fills with water, the proton concentration would fall, possibly allowing ATP to better activate P2XA Alternatively, regulation of ATP translocation could conceivably only allow ATP levels to reach the threshold concentration for P2XA activation only when vacuoles are ready to fuse[35]. However, this raises more questions as to the exact concentration of ATP in the CV, and the identity of the ATP transporter.

Many studies have highlighted the importance of calcium in the regulation of vesicle fusion events. They have revealed that calcium is released from the vacuole lumen and that required changes are localized and fast. Indeed, measurements using the P2XA-GCaMP2 sensor described in this study reveal that the calcium concentration around the CV increases almost two fold prior to fusion. We estimate this results in a localized calcium concentration of 100-200 nM, assuming basal cytoplasmic levels are 50-90 nM [44]. However, in many systems studies of the role of calcium changes have been hampered by the lack of available genetic tools. Most notably, identification of specific calcium channels responsible for release has proven elusive [7-19]. Our studies thus provide a significant advance as they reveal that activity of a calcium permeable ion channel within vesicles can affect vesicle fusion. Most importantly, we have also demonstrated a molecular mechanism by which calcium efflux through ion channels can regulate Rab dependent vesicle fusion events. Several lines of evidence suggest this is likely to represent a conserved mode of action. For example, the key principles and regulatory components of different intracellular vesicular trafficking mechanisms are broadly conserved at the molecular level. Most importantly, sequence comparisons reveal that the genomes of higher organisms contain several homologues of the calcium dependent Rab GAP, CnrF (Supplementary Figure 8), which represent good candidates for ion channel or calcium dependent regulation.

Understanding how the sequential activation of Rab GTPases is achieved during vesicle trafficking is a central question in cell biology. Several different solutions to this problem have been proposed. For example, in the Rab GEF cascade, activation of one Rab results in the recruitment of effectors, including the GEF for the downstream Rab [2, 45]. Counter

cascades of Rab GAP recruitment serve to amplify the cascade [4, 6, 46] or prevent premature activation of the next Rab in the cascade[47]. However, this in turn begs the question of how regulatory Rab GEFs or Rab GAPs are activated at the right place and time. Our studies thus provide one simple solution to this problem as they illustrate a mechanism by which a constitutively expressed Rab GAP can be temporally and spatially activated in order to correctly regulate the activity of one or more different Rabs to allow vesicle fusion.

Materials and Methods

Strains, culture and maintenance

Dictyostelium discoideum AX4 strains were grown and maintained in association with *Klebsiella aerogenes* or in HL5 axenic medium [48]. Transformants were selected in blasticidin (10 μg/ml) or G418 (20 μg/ml).

Plasmid construction

For deletion of the P2XA and putative Rab GAP genes, a floxed blasticidin cassette was cloned within genomic fragments flanking the coding sequence of each gene. Linearised construct was transformed into *AX4* cells by electroporation followed by blasticidin selection and confirmation of gene deletion by PCR. The blasticidin cassette was then removed by Cre recombinase. Point mutations in P2XA and cnrF were generated using Stratagene Quikchange® site-directed mutagenesis methodology. Primers containing base substitutions were designed and used to amplify genomic DNA by PCR.

Primer sequences used for mutagenesis:

hdP2XA R63A: ATCGGCAGCGTGGCCACCAGCCTGAAGG

hdP2XA R285K: AGCATCCACAGCAAACTGCTCTACAAGC

ddP2XA K67A: AGAACAAGTTTAGCGGGTCCAAATAC

ddP2XA K289A: AGATTACTTTATGCGCGTCATGGTATTCG

ddP2XA R63A: TGGTTCTGTTGCGACAAGTTTAAAAGG

ddP2XA R285K: CCATGACGTTTATAAAGGAGCTTCGAATGAATAC

CrnF EF hand1 E623Q: GATTTCACACAATTAATGTCTGG

CrnF EF2 hand2 D659Q: CTCAAAGAGTCAAATGAAGTTAATG

CrnF RabGAP TBC R270A: GACAAAGACATATCAGCAACGTTCCCTGGC

Mutated genomic coding sequences were then cloned downstream of a floxed blasticidin cassette, and terminator sequences were cloned upstream. Linearised construct was then transformed into *AX4* cells by electroporation followed by blasticidin selection and confirmation of gene mutation by PCR and sequencing. Mutated versions of P2XA were also cloned as C terminal translational fusions into pDM324 (RFP fusion), or a modified version of pDM324 in which RFP was replaced with GCaMP2 (GCaMP2 fusion). For *P2XA*$^{-}$ rescue construct generation, the entire P2XA coding sequence was cloned as a C terminal translational fusion into pDM323 (GFP) or pDM324 (RFP) and transformed into *P2XA*$^{-}$ cells. For *cnrF*$^{-}$ rescue construct generation, either the full length coding sequence (residues 1-670), a truncated version that does not contain the EF hands (residues 1-410), the full length with point mutation R270A to disrupt GAP activity, or the full length with point mutations E623Q/D659Q to disrupt the EF hands, was cloned as a C terminal translational fusion into pDM323 (GFP) or pDM324 (RFP) and transformed into *cnrF*$^{-}$ cells. For overexpression of Rab11a, Rab11a^{CA}, Rab11a^{DN} and Rab8a, coding sequences were cloned

as a C terminal translational fusion into pDM323 (GFP) or pDM324 (RFP) and transformed into *AX4* cells. Dajumin-GFP and Drainin-GFP constructs were provided by Thierry Soldati (University of Geneva) and Rab11a^{CA}, Rab11a^{DN}, GST-Disgorgin and GST-Rab11a constructs by Rick Firtel (UC San Diego).

Electrophysiology

Point mutations were generated in P2XA (in pcDNA3.1) described previously (Fountain *et al* 2007) for expression in HEK cells. For whole-cell patch clamp recordings HEK 293 cells were transiently transfected with 1μg/μl mutated P2XA plus 0.1 μg/μl enhanced GFP (EGFP) using Lipofectamine 2000 (Invitrogen) in accordance with the manufacturers instructions. Whole-cell patch recordings were made from HEK293 cells at room temperature (20-24 °C), 24 – 48 h after transfection. Cells were voltage-clamped at −60 mV, and membrane currents amplified with a HEKA amplifier running Pulse and Pulsefit software (v 8.54; HEKA, USA). ATP was applied using an RSC 200 system (Biological Science Instruments) for 2 s duration at 2 min intervals and concentration-response curves for ATP were generated using either an ascending or a descending order of concentration. All data were analyzed using PulseFit and GraphPad Prism (GraphPad, USA) software. Numerical data are presented as mean ± s.e.m. The extracellular solution contained (in mM): 145 NaCl, 2 KCl, 2 CaCl2, 1 MgCl2, 13 D-glucose and 10 HEPES pH 7.3. For whole-cell recordings, the intracellular patch pipette solution contained (in mM): 145 NaCl, 10 HEPES and 10 EGTA, pH 7.3.

Osmoregulation assay

Wild-type or mutant cells were initially maintained in HL5 growth medium on glass bottomed imaging dishes before growth medium was replaced with distilled water. Adherent cells were imaged with an inverted Olympus IX71 microscope (63x objective); images were captured at 5-10 minute intervals with Simple PCI software (C-Imaging Systems). Circularity was measured offline for 70-120 cells per time point using ImageJ software. Numerical data are presented as means ± s.e.m.

Fluorescence Imaging

Cells expressing RFP and/or GFP constructs were maintained in glass-bottomed imaging dishes in HL5 growth medium at 22 °C. Adherent cells were imaged with an inverted Olympus IX71 microscope (63x objective); images were captured at 1-min intervals with Simple PCI software (C-Imaging Systems). Cell fluorescence intensity was measured in ImageJ by measuring integrated density normalised to cell area. For measurements of GCaMP2 fluorescence during CV cycling, ImageJ software was used to select a R.O.I. around a contractile vacuole, the total vacuole fluorescence for both GFP and RFP was then measured as described. GFP fluorescence was then normalized to RFP fluorescence.

Identification of P2XA-interacting proteins

For identification of interacting proteins, GFP-Trap (ChromoTek) was employed. A total of 3×10^7 cells expressing either GFP or P2XA-GFP were lysed in 250 μl buffer (50mM Tris HCl, 0.5% triton, 2mM $MgCl_2$, 150mM NaCl, supplemented with protease inhibitor (Complete; Roche)). The lysate was centrifuged for 15 min at 16,000 ×*g* and 75 μl of supernatant was incubated with 15 μl GFP-Trap agarose beads under slight agitation for 1 h at 4°C. The beads were washed according to the manufacturer's protocol, and bound proteins were eluted by boiling in SDS sample buffer. Proteins were separated by SDS–PAGE and stained with Coomassie brilliant blue-R. For protein identification, bound proteins were run into the top of an SDS– PAGE gel, excised and then analyzed *en masse* by

in-house mass spectrometry using the Waters Q-TOF Micro with Waters CapLC chromatography system after overnight trypsination.

Rab11a-GTP measurement assay

Rab11a activity was measured in all strains using a conformation specific antibody that specifically recognizes Rab11-GTP (NewEast Biosciences catalogue number 26919). For *in vitro* precipitation of Rab11a-GTP, 1 μg bacterially expressed GST Rab was incubated with 20mM EDTA and either 100 μM GTPγS or 1 mM GDP for 30 minutes at 30°C. GTP/GDP loading was stopped by placing the tubes on ice and adding 60 mM $MgCl_2$. Reaction volume was adjusted to 1 ml with lysis buffer (50 mM Tris-HCl, pH 8, 150 mM NaCl, 10 mM $MgCl_2$, 1 mM EDTA, 1% Triton X-100) before incubating with 1 μl of anti Rab11-GTP antibody and 20 μl of protein A/G agarose (50% slurry) for 1 hour at 4°C with gentle agitation. Beads were washed three times in lysis buffer before elution of bound protein by boiling in 20 μl of 2X SDS sample buffer. Proteins were separated by SDS-PAGE and immunoblotted for GST using an anti-GST antibody (Abcam catalogue number ab6613). For *in vivo* precipitation of rab11a-GTP, 1×10^7 cells expressing Rab11a-RFP were lysed in 1ml lysis buffer (50 mM Tris-HCl, pH 8, 150 mM NaCl, 10 mM $MgCl_2$, 1 mM EDTA, 1% Triton X-100). Lysate was then incubated with 1 μl of anti Rab11-GTP antibody and 20 μl of protein A/G agarose (50% slurry) for 1 hour at 4°C with gentle agitation. Beads were washed three times in lysis buffer before elution of bound protein by boiling in 20 μl of 2X SDS sample buffer. Proteins from input, bound and not bound fractions were separated by SDS-PAGE and immunoblotted for RFP using an anti-RFP antibody (Chromotek catalogue number 3F5). Anti-actin antibody (Santa Cruz Biotechnology catalogue number sc-47778) was used as a loading control for each sample. The ratio of bound Rab11a-RFP (Rab11a-GTP) and unbound Rab11a-RFP (Rab11a-GDP) was calculated for each clone after normalizing against the actin loading control. Densitometry analyses of western blots was performed in imageJ. All blots analysed were in the linear range.

GST pull-down and GAP assays

GST-fused proteins were expressed in BL21(DE3) bacteria and purified on glutathione-sepharose beads. GAP assays were performed as previously described in [22, 37]. Briefly, 10 nM or 100 nM GAPs were incubated in the presence of 2.5 μM purified Rab pre-loaded with GTP. The amount of released inorganic phosphate was measured using the EnzChek Phosphate Assay Kit (Invitrogen) in 96 well plates according to the manufacturers instructions. Changes in absorbance were measured at 360 nm using a BioTek Synergy HT plate reader. Five technical and three independent biological replicates were performed. For GST pulldowns from *Dictyostelium* cell lysates [22, 49], *AX4* cells expressing Rab11-RFP, Rab8-RFP or P2XA-RFP were incubated at 4°C for 1hr with 10 μg of GST–GAP bound to glutathione-agarose beads. After washing the beads three times, bound proteins were eluted by boiling in SDS sample buffer. Eluted proteins were run on SDS–PAGE gel and probed with anti-RFP antibody (Chromotek catalogue number 3F5).

Supplementary Material

Refer to Web version on PubMed Central for supplementary material.

Acknowledgments

This work was supported by a Medical Research Council grant (G0900069) to RAN and CRLT and a Wellcome Trust Investigator Award (WT095643) to CRLT.

References

1. Hutagalung AH, Novick PJ. Role of Rab GTPases in membrane traffic and cell physiology. Physiol Rev. 2011; 91:119–149. [PubMed: 21248164]
2. Lippe R, Miaczynska M, Rybin V, Runge A, Zerial M. Functional synergy between Rab5 effector Rabaptin-5 and exchange factor Rabex-5 when physically associated in a complex. Mol Biol Cell. 2001; 12:2219–2228. [PubMed: 11452015]
3. Mizuno-Yamasaki E, Medkova M, Coleman J, Novick P. Phosphatidylinositol 4-phosphate controls both membrane recruitment and a regulatory switch of the Rab GEF Sec2p. Dev Cell. 2010; 18:828–840. [PubMed: 20493815]
4. Ortiz D, Medkova M, Walch-Solimena C, Novick P. Ypt32 recruits the Sec4p guanine nucleotide exchange factor, Sec2p, to secretory vesicles; evidence for a Rab cascade in yeast. J Cell Biol. 2002; 157:1005–1015. [PubMed: 12045183]
5. Pereira-Leal JB, Seabra MC. Evolution of the Rab family of small GTP-binding proteins. J Mol Biol. 2001; 313:889–901. [PubMed: 11697911]
6. Mizuno-Yamasaki E, Rivera-Molina F, Novick P. GTPase networks in membrane traffic. Annu Rev Biochem. 2012; 81:637–659. [PubMed: 22463690]
7. Hay JC. Calcium: a fundamental regulator of intracellular membrane fusion? EMBO Rep. 2007; 8:236–240. [PubMed: 17330068]
8. Adler EM, Augustine GJ, Duffy SN, Charlton MP. Alien intracellular calcium chelators attenuate neurotransmitter release at the squid giant synapse. J Neurosci. 1991; 11:1496–1507. [PubMed: 1675264]
9. Beckers CJ, Balch WE. Calcium and GTP: essential components in vesicular trafficking between the endoplasmic reticulum and Golgi apparatus. J Cell Biol. 1989; 108:1245–1256. [PubMed: 2538479]
10. Burgoyne RD, Clague MJ. Calcium and calmodulin in membrane fusion. Biochim Biophys Acta. 2003; 1641:137–143. [PubMed: 12914954]
11. Colombo MI, Beron W, Stahl PD. Calmodulin regulates endosome fusion. J Biol Chem. 1997; 272:7707–7712. [PubMed: 9065429]
12. Holroyd C, Kistner U, Annaert W, Jahn R. Fusion of endosomes involved in synaptic vesicle recycling. Mol Biol Cell. 1999; 10:3035–3044. [PubMed: 10473644]
13. Peters C, Mayer A. Ca2+/calmodulin signals the completion of docking and triggers a late step of vacuole fusion. Nature. 1998; 396:575–580. [PubMed: 9859992]
14. Porat A, Elazar Z. Regulation of intra-Golgi membrane transport by calcium. J Biol Chem. 2000; 275:29233–29237. [PubMed: 10871627]
15. Pryor PR, Mullock BM, Bright NA, Gray SR, Luzio JP. The role of intraorganellar Ca(2+) in late endosome-lysosome heterotypic fusion and in the reformation of lysosomes from hybrid organelles. J Cell Biol. 2000; 149:1053–1062. [PubMed: 10831609]
16. Chen JL, Ahluwalia JP, Stamnes M. Selective effects of calcium chelators on anterograde and retrograde protein transport in the cell. J Biol Chem. 2002; 277:35682–35687. [PubMed: 12114519]
17. Flanagan JJ, Barlowe C. Cysteine-disulfide cross-linking to monitor SNARE complex assembly during endoplasmic reticulum-Golgi transport. J Biol Chem. 2006; 281:2281–2288. [PubMed: 16303754]
18. Starai VJ, Thorngren N, Fratti RA, Wickner W. Ion regulation of homotypic vacuole fusion in Saccharomyces cerevisiae. J Biol Chem. 2005; 280:16754–16762. [PubMed: 15737991]
19. Xu D, Hay JC. Reconstitution of COPII vesicle fusion to generate a pre-Golgi intermediate compartment. J Cell Biol. 2004; 167:997–1003. [PubMed: 15611329]
20. Becker M, Matzner M, Gerisch G. Drainin required for membrane fusion of the contractile vacuole in Dictyostelium is the prototype of a protein family also represented in man. EMBO J. 1999; 18:3305–3316. [PubMed: 10369671]
21. Bush J, Temesvari L, Rodriguez-Paris J, Buczynski G, Cardelli J. A role for a Rab4-like GTPase in endocytosis and in regulation of contractile vacuole structure and function in Dictyostelium discoideum. Mol Biol Cell. 1996; 7:1623–1638. [PubMed: 8898366]

22. Du F, et al. Regulation of contractile vacuole formation and activity in Dictyostelium. EMBO J. 2008; 27:2064–2076. [PubMed: 18636095]
23. Essid M, Gopaldass N, Yoshida K, Merrifield C, Soldati T. Rab8a regulates the exocyst-mediated kiss-and-run discharge of the Dictyostelium contractile vacuole. Mol Biol Cell. 2012; 23:1267–1282. [PubMed: 22323285]
24. Gerald NJ, Siano M, De Lozanne A. The Dictyostelium LvsA protein is localized on the contractile vacuole and is required for osmoregulation. Traffic. 2002; 3:50–60. [PubMed: 11872142]
25. Harris E, Yoshida K, Cardelli J, Bush J. Rab11-like GTPase associates with and regulates the structure and function of the contractile vacuole system in dictyostelium. J Cell Sci. 2001; 114:3035–3045. [PubMed: 11686306]
26. Heuser J, Zhu Q, Clarke M. Proton pumps populate the contractile vacuoles of Dictyostelium amoebae. J Cell Biol. 1993; 121:1311–1327. [PubMed: 8509452]
27. Wu WI, Yajnik J, Siano M, De Lozanne A. Structure-function analysis of the BEACH protein LvsA. Traffic. 2004; 5:346–355. [PubMed: 15086784]
28. Moreno SN, Docampo R. The role of acidocalcisomes in parasitic protists. J Eukaryot Microbiol. 2009; 56:208–213. [PubMed: 19527347]
29. Bos JL, Rehmann H, Wittinghofer A. GEFs and GAPs: critical elements in the control of small G proteins. Cell. 2007; 129:865–877. [PubMed: 17540168]
30. Gerisch G, Heuser J, Clarke M. Tubular-vesicular transformation in the contractile vacuole system of Dictyostelium. Cell Biol Int. 2002; 26:845–852. [PubMed: 12421575]
31. Fountain SJ, et al. An intracellular P2X receptor required for osmoregulation in Dictyostelium discoideum. Nature. 2007; 448:200–203. [PubMed: 17625565]
32. Khakh BS, North RA. Neuromodulation by extracellular ATP and P2X receptors in the CNS. Neuron. 2012; 76:51–69. [PubMed: 23040806]
33. Surprenant A, North RA. Signaling at purinergic P2X receptors. Annu Rev Physiol. 2009; 71:333–359. [PubMed: 18851707]
34. Baines A, et al. Functional properties of five Dictyostelium discoideum P2X receptors. J Biol Chem. 2013
35. Sivaramakrishnan V, Fountain SJ. A mechanism of intracellular P2X receptor activation. J Biol Chem. 2012; 287:28315–28326. [PubMed: 22736763]
36. Richler E, Chaumont S, Shigetomi E, Sagasti A, Khakh BS. Tracking transmitter-gated P2X cation channel activation in vitro and in vivo. Nature methods. 2008; 5:87–93. [PubMed: 18084300]
37. Pan X, Eathiraj S, Munson M, Lambright DG. TBC-domain GAPs for Rab GTPases accelerate GTP hydrolysis by a dual-finger mechanism. Nature. 2006; 442:303–306. [PubMed: 16855591]
38. Starovasnik MA, Su DR, Beckingham K, Klevit RE. A series of point mutations reveal interactions between the calcium-binding sites of calmodulin. Protein science : a publication of the Protein Society. 1992; 1:245–253. [PubMed: 1363934]
39. Miklavc P, et al. Fusion-activated Ca2+ entry via vesicular P2X4 receptors promotes fusion pore opening and exocytotic content release in pneumocytes. Proc Natl Acad Sci U S A. 2011; 108:14503–14508. [PubMed: 21844344]
40. Qureshi OS, Paramasivam A, Yu JC, Murrell-Lagnado RD. Regulation of P2X4 receptors by lysosomal targeting, glycan protection and exocytosis. J Cell Sci. 2007; 120:3838–3849. [PubMed: 17940064]
41. Ludlow MJ, Durai L, Ennion SJ. Functional characterization of intracellular Dictyostelium discoideum P2X receptors. J Biol Chem. 2009; 284:35227–35239. [PubMed: 19833731]
42. Temesvari LA, Rodriguez-Paris JM, Bush JM, Zhang L, Cardelli JA. Involvement of the vacuolar proton-translocating ATPase in multiple steps of the endo-lysosomal system and in the contractile vacuole system of Dictyostelium discoideum. J Cell Sci. 1996; 109(Pt 6):1479–1495. [PubMed: 8799835]
43. Allen RD. The contractile vacuole and its membrane dynamics. Bioessays. 2000; 22:1035–1042. [PubMed: 11056480]
44. Allan CY, Fisher PR. In vivo measurements of cytosolic calcium in Dictyostelium discoideum. Methods in molecular biology. 2009; 571:291–308. [PubMed: 19763975]

45. Guo W, Roth D, Walch-Solimena C, Novick P. The exocyst is an effector for Sec4p, targeting secretory vesicles to sites of exocytosis. EMBO J. 1999; 18:1071–1080. [PubMed: 10022848]
46. Medkova M, France YE, Coleman J, Novick P. The rab exchange factor Sec2p reversibly associates with the exocyst. Mol Biol Cell. 2006; 17:2757–2769. [PubMed: 16611746]
47. Chesneau L, et al. An ARF6/Rab35 GTPase cascade for endocytic recycling and successful cytokinesis. Current biology : CB. 2012; 22:147–153. [PubMed: 22226746]
48. Sussman M. Cultivation and synchronous morphogenesis of Dictyostelium under controlled experimental conditions. Methods Cell Biol. 1987; 28:9–29. [PubMed: 3298997]
49. Sasaki AT, Chun C, Takeda K, Firtel RA. Localized Ras signaling at the leading edge regulates PI3K, cell polarity, and directional cell movement. J Cell Biol. 2004; 167:505–518. [PubMed: 15534002]

Europe PMC Funders Author Manuscripts

Europe PMC Funders Author Manuscripts

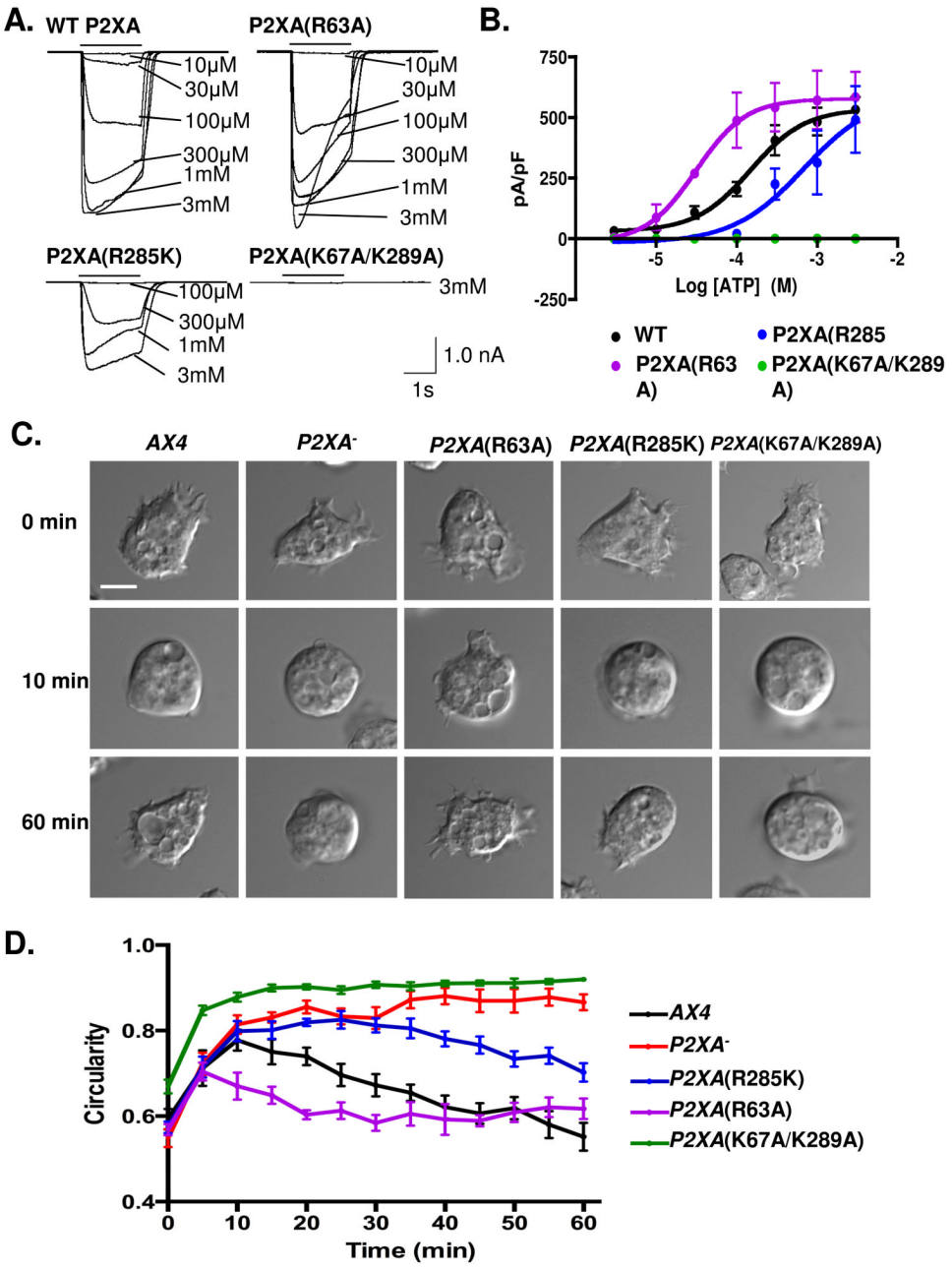

Figure 1. P2XA mutants with altered ATP sensitivity show defects in osmoregulation

A. Currents evoked by ATP (10 μM - 3 mM) in HEK cells expressing wild type (WT) or mutated P2XA receptors. Each panel shows superimposed current traces for the concentrations indicated. ATP application was 2 s (black bar). B. Concentration-response curves for wild type (black), R285K (blue), R63A (purple) and K67A/K289A (green) receptors. Error bars represent s.e.m. of responses from wild type (8 cells), R285K (4 cells), R63A (4 cells) and K67A/K289A (3 cells). Compared to WT–P2XA (black), concentration response curves for R63A (purple) are shifted left ($p<0.001$ in a tukey test), whilst R285K (blue) is shifted right ($p<0.001$ in a tukey test). K67A/K289A (green) is non-functional ($p<0.0001$ in a tukey test). Statistical source data for Fig 1B can be found in Supplementary

Table 2. C. Bright-field images of *Dictyostelium AX4* cells in KK2 (0 min), and at 10 and 60 min after changing the solution to water. Scale bar = 5 μm. D. Time course of cell increase in circularity, and recovery. Wild-type cells (black) round up for 10-15 min and then regain their normal shape by 40 min. *P2XA*$^{-}$ cells (red) stay round throughout the entire time course. A paired T test between *P2XA*$^{-}$ and wild type revealed no significant differences at 0 and 10 min ($p=0.72$) but significantly different ($p<0.0001$) behavior throughout the rest of the cycle. P2XA(R63A) cells (purple) initially round up, however they fully recover their shape significantly more quickly than wild type ($p<0.001$ at 20 min). Both P2XA(R285K) (blue) and P2XA(K67A/K289A) (green) round up within 10 min, P2XA(K67A/K289A) remains round and is not significantly different to *P2XA*$^{-}$ cells throughout the cycle ($p=0.84$), whilst P2XA(R285K) is able to partially recover to an intermediate phenotype that is significantly different from both wild type ($p<0.001$ at 60 minutes) and *P2XA*$^{-}$ cells ($p<0.001$ at 60 minutes). Error bars represent s.e.m. and results are means of n=4 independent experiments, each with 70 cells. Statistical source data for Fig 1D can be found in Supplementary Table 2.

Europe PMC Funders Author Manuscripts

Europe PMC Funders Author Manuscripts

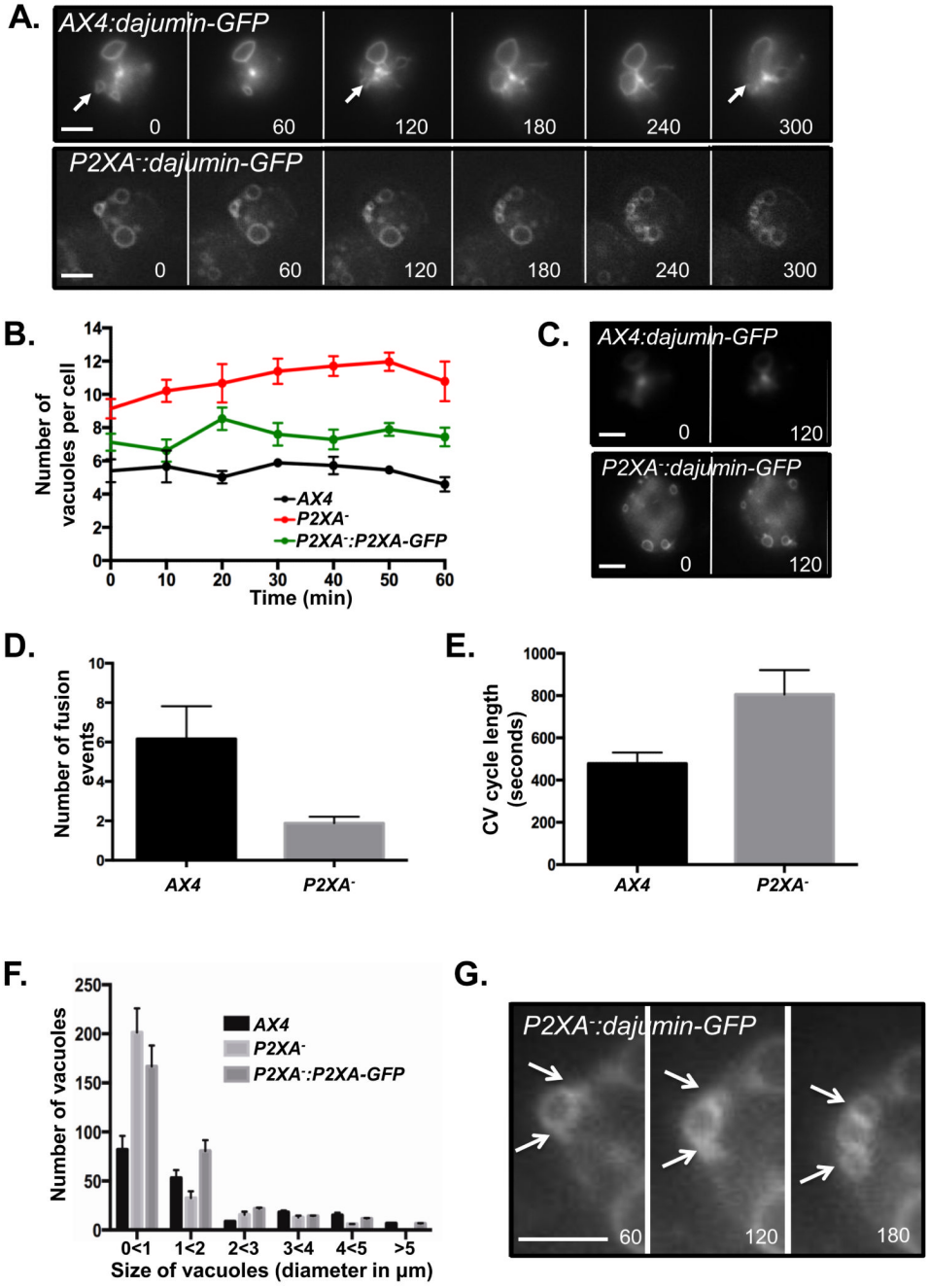

Figure 2. P2XA⁻ cells exhibit aberrant contractile vacuole number, dynamics and morphology

A. Fluorescence images of wild-type and *P2XA*⁻ cells expressing Dajumin-GFP during CV cycling. Closed arrows indicate points in the CV cycle where a CV fuses to the plasma membrane and water is expelled. Numbers represent the time in seconds after changing the media from KK2 to water. Scale bar = 5μm. B. *P2XA*⁻ cells have more vacuoles per cell than wild-type. *P2XA*⁻ cells overexpressing *P2XA:GFP* have slightly more vacuoles per cell than wild-type, but fewer than *P2XA*⁻ cells. Error bars represent s.e.m. and results are means of n=3 independent experiments, each with 50 cells. Statistical source data for Fig 2B can be found in Supplementary Table 2.C. Fluorescence images of wild-type and P2XA⁻ cell expressing Dajumin-GFP taken within the plane of the middle of the cell. Numbers

represent the time in seconds after changing the media from KK2 to water. Scale bar = 5μm. D. The vacuoles in *P2XA*-cells undergo far fewer fusion/expulsion events than wild-type vacuoles during the time course. Error bars represent s.e.m. and results are means of n=3 independent experiments, each with 50 cells. Statistical source data for Fig 2D can be found in Supplementary Table 2. E. The time taken for a CV to complete a cycle was twice as long for a *P2XA*$^{-}$ vacuole compared to wild-type vacuoles. Error bars represent s.e.m. and results are means of n=3 independent experiments, each with 50 vacuoles. Statistical source data for Fig 2E can be found in Supplementary Table 2.F. *P2XA*-cells have larger numbers of small vacuoles than wild-type cells, and very few bigger vacuoles. *P2XA*$^{-}$ cells overexpressing *P2XA:GFP* have more small vacuoles than wild-type cells, but the number of bigger vacuoles is similar to wild-type cells. Error bars represent s.e.m. and results are means of n=3 independent experiments, each with 50 cells. Statistical source data for Fig 2F can be found in Supplementary Table 2.G. Zoom of fluorescence images of *P2XA*$^{-}$ cell from panel A expressing Dajumin-GFP. White arrows indicate a “budding” vacuole.

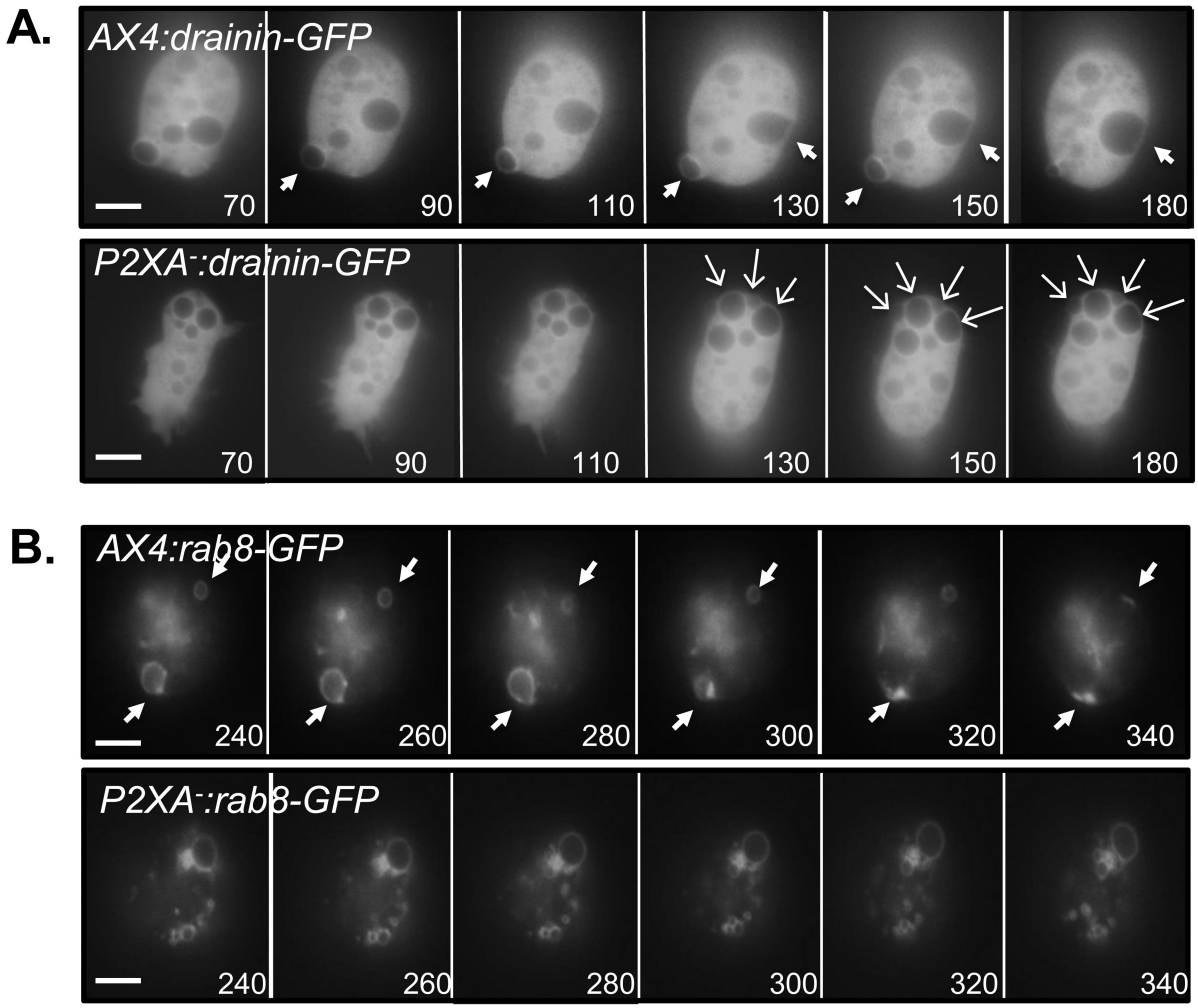

Figure 3. P2XA⁻ cells fail to undergo the ring-to-patch transition stage of the CV cycle

A. Fluorescence images of a wild-type and *P2XA*⁻ cells expressing Drainin-GFP. Closed white arrows indicate vacuoles at the 'ring to patch' transition stage. In *P2XA*-cells, Drainin-GFP becomes recruited to CV's as they mature. However, Drainin-GFP localization does not change and 'ring to patch' transition is not observed. Open arrows indicate vacuoles that have reached the stage where 'ring to patch' transition should occur. B. Fluorescence images of wild-type and *P2XA*⁻ cells expressing Rab8a-GFP. Closed white arrows indicate a vacuole at the 'ring to patch' transition stage. In *P2XA*⁻ cells, Rab8a-GFP becomes recruited to mature CV's. However, Rab8a-GFP localization does not change and 'ring to patch' transition is not observed. Numbers represent the time in seconds after changing the media from KK2 to water. Scale bars = 5μm.

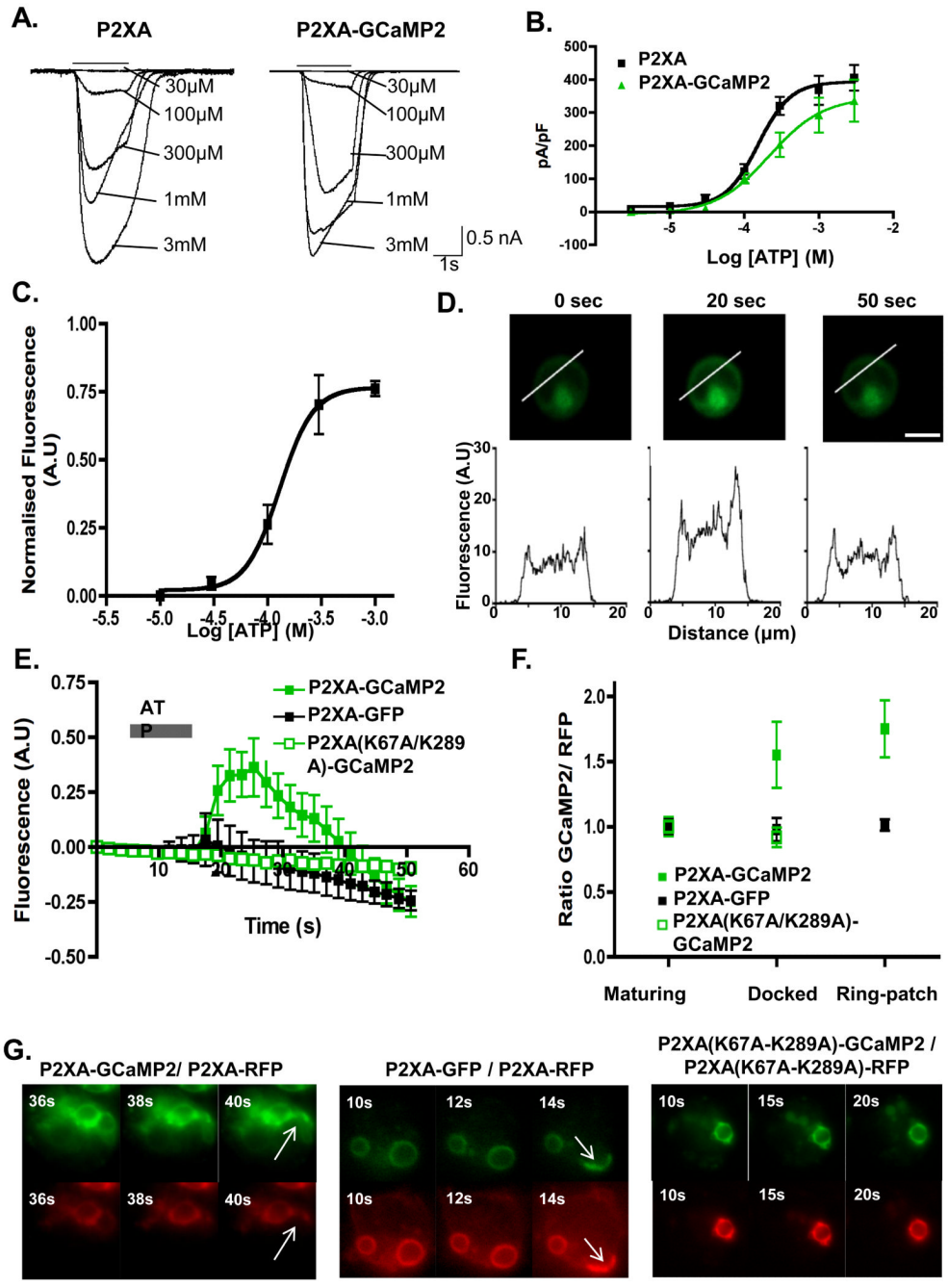

Figure 4. GCaMP2 sensor indicates that P2XA activity is increased in docked vesicles

A. Currents evoked by ATP (black bar, concentrations indicated) in HEK cells expressing P2XA (*left*) or P2XA-GCaMP2 (*right*) receptors. B. Concentration-response curves for HEK cells expressing wild type (black) or (green) P2XAGCaMP2 receptors shows no significant difference in sensitivity to ATP. Error bars represent s.e.m. and results are means from n=21 wild type and n=7 P2XA-GCaMP expressing cells. C. Concentration-response curve for GCaMP2 fluorescence in HEK cells expressing P2XA-GCaMP2. Ordinate is normalized to the maximal fluorescence observed with ATP. Effective concentrations of ATP are similar to those in B (Error bars represent s.e.m. and results are means from n=7 cells). D. Line scans from HEK cells expressing P2XA-GCaMP2 at 0, 20 and 50 s after ATP application

shows increased fluorescence at plasma membrane. Scale bar = 10 μm. E. ATP (1 mM) increases GCaMP2 fluorescence in cells expressing wild type P2XA receptors (filled green squares), but not in cells expressing P2XA(K67A/K289A) receptors (open green squares) or P2XA-GFP receptors (black squares). Error bars represent s.e.m. and results are means from n=6 cells). F. *Dictyostelium* cells co-expressing P2XA-RFP and either P2XA-GCaMP2 (filled green squares), P2XA(K67A/K289A)-GCaMP2 (open green squares), or P2XA-GFP (filled black squares) were subjected to osmotic shock. The ratio of GFP to RFP fluorescence was measured at three stages throughout the cycle (maturing, docked, and ring-to-patch) for each strain (except cells expressing P2XA(K67A/K289A)-GCaMP2 receptors were not studied at ring-to-patch stage because these cells do not undergo that stage). The GFP/RFP ratio in cells expressing P2XA-GCaMP2 increased significantly at the later stages of the CV cycle (paired t test between P2XA-GCaMP2/ P2XA-RFP and P2XA-GFP/P2XA-RFP gives $p<0.001$ at both docked and ring-to-path stages). In cells expressing P2XA9K67A/K289A)-GCaMP2 or P2XA-GFP the GFP/RFP ratio remained constant throughout the cycle (Error bars represent s.e.m. and results are means from n=10 cells). G. Fluorescence images of *Dictyostelium* cells co-expressing P2XA-GCaMP2 and P2XA-RFP, P2XA-GFP and P2X-RFP or P2XA(K67A/K289A)-GCaMP2 and P2XA(K67A/K289A)-RFP during osmoregulation. Arrows indicate ‘ring to patch’ transition of P2XA and fusion events. Scale bar = 5μm.

Europe PMC Funders Author Manuscripts

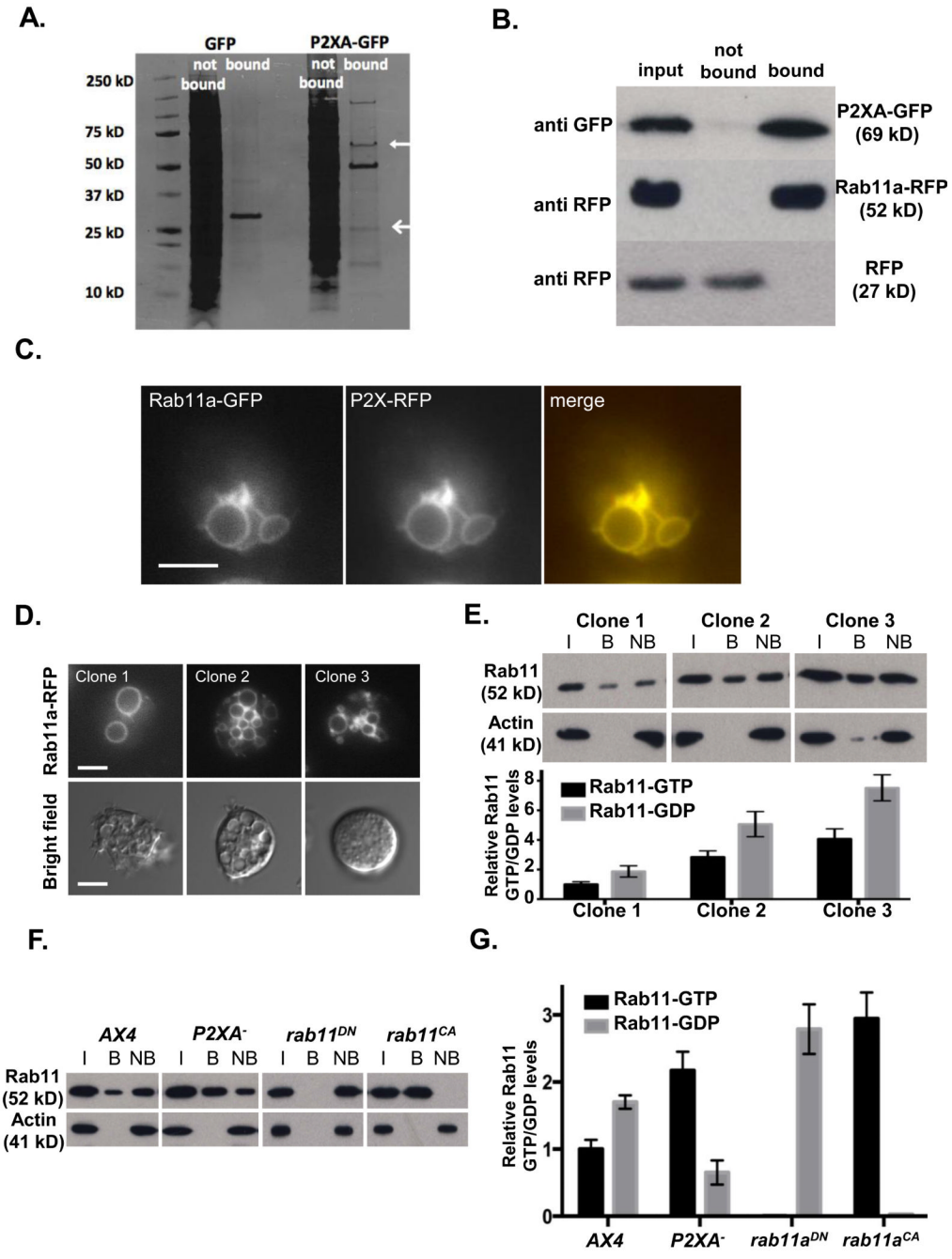

Figure 5. P2XA suppresses Rab11a activity

A. Immunoprecipitation of GFP or P2XA-GFP from wild-type cells. P2XA is indicated with a closed arrow, Rab11a is indicated with an open arrow. B. Immunoprecipitation of Rab11a-RFP or RFP from P2XA-GFP co-expressing cells. Lysates were incubated with anti-GFP beads and input, bound and not bound fractions probed with either anti-GFP or anti-RFP antibodies. C. Localization of P2XA-RFP and Rab11a-GFP in wild-type cells. P2XA and Rab11a co-localize on the CV. D. Overexpression of Rab11a-RFP results in osmoregulation defects similar to those observed for *P2XA*$^{-}$ cells. Quantification of fluorescence levels in three clones (clone 1 = 1052 A.U., clone 2 = 2183 A.U., clone 3 = 4911 A.U.) shows that higher expression results in more small vacuoles that fail to fuse (top panel) and less

Europe PMC Funders Author Manuscripts

recovery from osmotic shock (bottom panel). E. Quantification of Rab11a-GTP levels in the three Rab11a-RFP expressing clones by immunoprecipitation with a Rab11a-GTP specific antibody as described in Materials and Methods (I = input, B = bound, NB = not bound). A paired T test revealed that the ratio of GTP and GDP bound Rab11a was not significantly different between the three clones (p=0.89 for each pair). Error bars represent s.e.m. from n=3 three independent experiments. Statistical source data for Fig 5E can be found in Supplementary Table 2.F. Immunoprecipitation of Rab11a-GTP from *AX4* cells expressing Rab11a-RFP, *P2XA*$^{-}$ cells expressing Rab11a-RFP, wild type cells expressing dominant negative Rab11a [22] fused to RFP, and wild type cells expressing constitutively active Rab11a [22] fused to RFP. The level of Rab11a-RFP expression (input) is comparable between all strains (>1.25 fold difference between highest and lowest). G. Quantification of GTP and GDP bound Rab11a . A paired T test revealed a significant increase (2.2 fold) in the levels of GTP bound Rab11a in *P2XA*$^{-}$ cells compared to wild type cells (p<0.001). Wild type cells expressing a dominant negative form of Rab11a have undetectable levels of GTP bound Rab11a, whereas wild type cells expressing a constitutively active form of Rab11a have the majority of Rab11a in a GTP bound state, with only very low levels of Rab11a bound to GDP. Error bars represent s.e.m. from n=3 three independent experiments. Statistical source data for Fig 5G can be found in Supplementary Table 2.

Europe PMC Funders Author Manuscripts

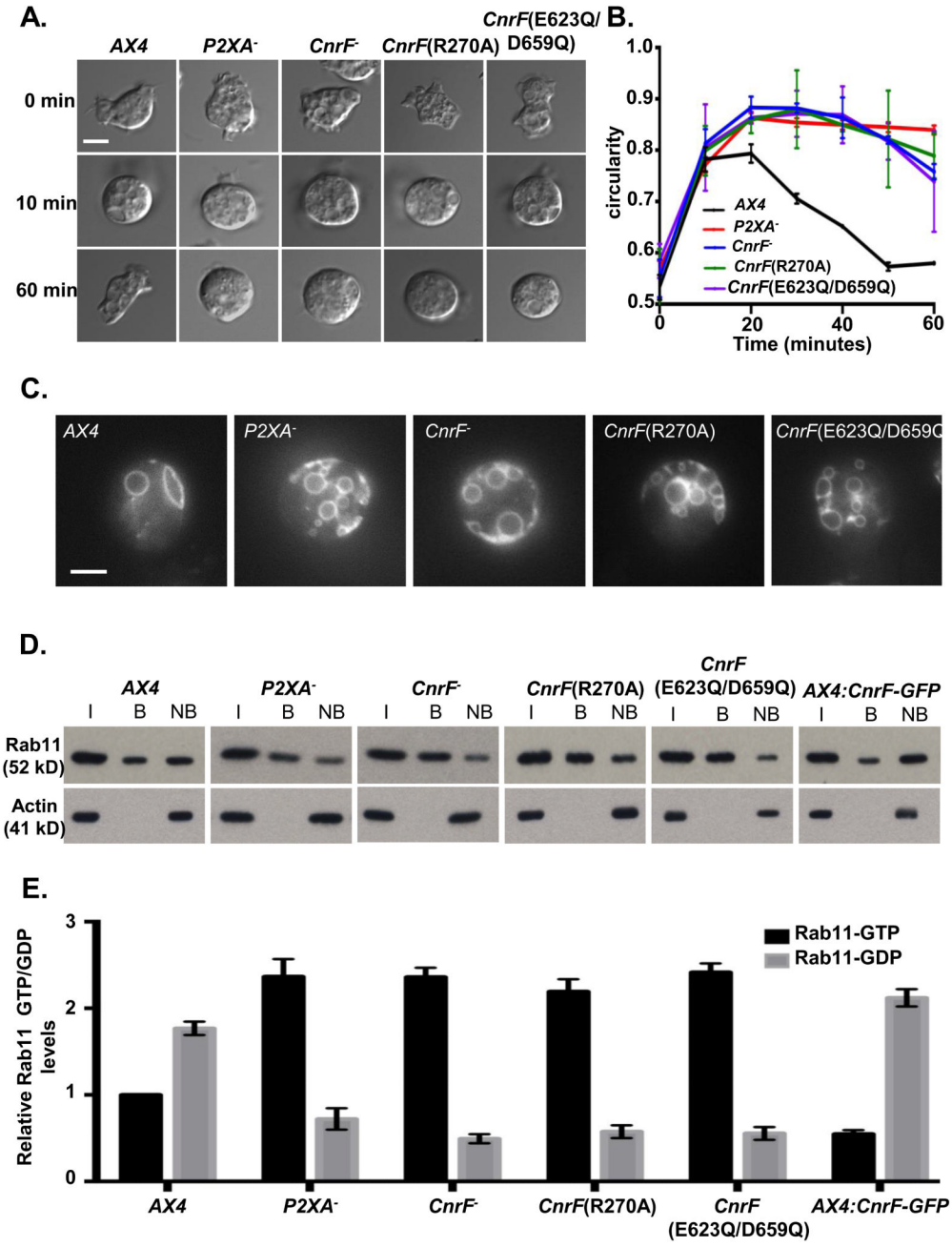

Figure 6. cnrF is required for normal osmoregulation and regulation of Rab11 activity

A. *cnrF* mutant cells exhibit impaired osmoregulation. Representative bright-field images of cells in KK2, and after 10 min and 60 min after changing the media from KK2 to water to induce osmotic shock. Scale bar = 5μm. B. Time course of cell rounding and recovery. *cnrF*$^{-}$, *cnrF*(R270A) and *cnrF*(E623Q/D659Q) mutant cells exhibit similar osmoregulation defects to *P2XA*$^{-}$ cells. Error bars represent s.e.m. from n=3 three independent experiments, each with 100 cells. Statistical source data for Fig 6B can be found in Supplementary Table 2. C. Visualisation of CV morphology in wild-type, *P2XA*$^{-}$ *cnrF*$^{-}$, *cnrF*(R270A) or *cnrF*(E623Q/D659Q) cells expressing Dajumin-GFP after osmotic shock .All *cnrF* mutants contain many irregularly sized vacuoles at the cell surface that fail to fuse. Scale bar = 5μm.

Europe PMC Funders Author Manuscripts

D and E. Immunoprecipitation of Rab11a-GTP from wild-type, *P2XA*$^{-}$ *cnrF*$^{-}$, *cnrF*(R270A), *cnrF*(E623Q/D659Q) and CnrF-GFP overexpressing cells expressing Rab11a-RFP (I = input, B = bound, NB = not bound). The level of Rab11a-RFP expression (input) is comparable between all strains (>1.3 fold difference between highest and lowest). E. Quantification of GTP and GDP bound Rab11a revealed that all mutant strains exhibit a significant (paired T test $p<0.001$) 2-2.5 fold increase in the levels of Rab11a-GTP compared to wild type cells. Furthermore CnrF-GFP overexpressing cells exhibit a reciprocal 2 fold decrease in GTP bound Rab11a compare to wild type (paired T test $p<0.001$). Error bars represent s.e.m. from n=3 three independent experiments. Statistical source data for Fig 6E can be found in Supplementary Table 2.

Europe PMC Funders Author Manuscripts

Europe PMC Funders Author Manuscripts

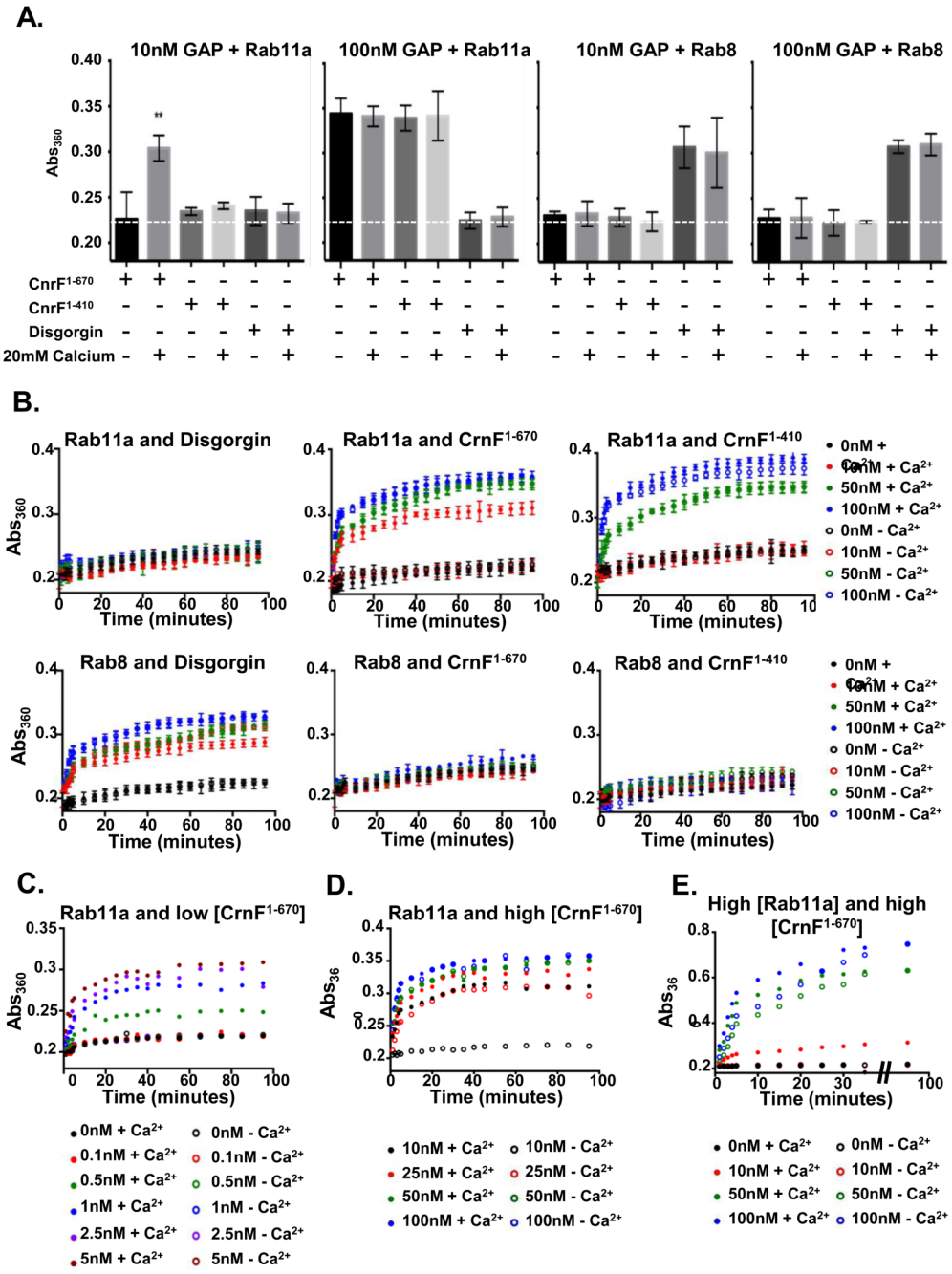

Figure 7. cnrF encodes a calcium sensitive Rab11a GAP

A. GTP hydrolysis of Rab11a or Rab8a by bacterially expressed CnrF. Rabs were incubated with 10nM or 100nM GST-CnrF$^{1-670}$ (full length), GST-CnrF$^{1-410}$ (truncation which removes EF hands) or GST-disgorgin$^{382-717}$ in the presence or absence of 20 mM calcium. When putative GAPs were incubated at 10nM, GSTCnrF$^{1-670}$ shows significant Rab11a-GTP hydrolysis, but only in the presence of 20 mM calcium (Paired T test $p<0.001$). When putative GAPs were incubated at 100nM, both GST-CnrF$^{1-670}$ and GST-CnrF$^{1-410}$ show significant Rab11a-GTP hydrolysis. The addition of 20 mM calcium has no significant effect (Paired T test $p=0.87$). Only GST-disgorgin$^{382-717}$ shows significant Rab8 hydrolysis (Paired T test $p<0.001$), which is unaffected by the addition of 20 mM calcium (Paired T test

p=0.83). The dashed line represents the mean Abs_{360} when 0nM GAP is added (S.E.M. = 0.00423). Error bars represent s.e.m. from n=3 three independent experiments, each with five technical replicates. B. Time courses of Rab11a-GTP or Rab8-GTP hydrolysis with 0, 10, 50 or 100nM GAPs. Error bars represent s.e.m. from n=3 three independent experiments, each with five technical replicates. C. Calcium dependent Rab11a-GTP hydrolysis is observed at a wide range of GST-$CnrF^{1-670}$ concentrations (0.5-5 nM). Results are means of 2 independent experiments, each with three technical replicates. D. In the presence of rate limiting amounts of Rab11a-GTP (2.5μM) GST-$CnrF^{1-670}$ exhibits significant levels of calcium independent Rab11a-GTP hydrolysis. Results are means of 2 independent experiments, each with three technical replicates. E. When Rab11a is present at a non-limiting concentration (25μM, 10x higher than that used in A-C), the presence of 20mM calcium increases the rate of Rab11a hydrolysis by both 50nM and 100nM GST-$CnrF^{1-670}$. These results suggest that calcium can increase the efficiency of Rab11a hydrolysis by GST-$CnrF^{1-670}$ at all GAP concentrations tested. Results are means of 2 independent experiments, each with three technical replicates. Statistical source data for Fig 7A-E can be found in Supplementary Table 2.

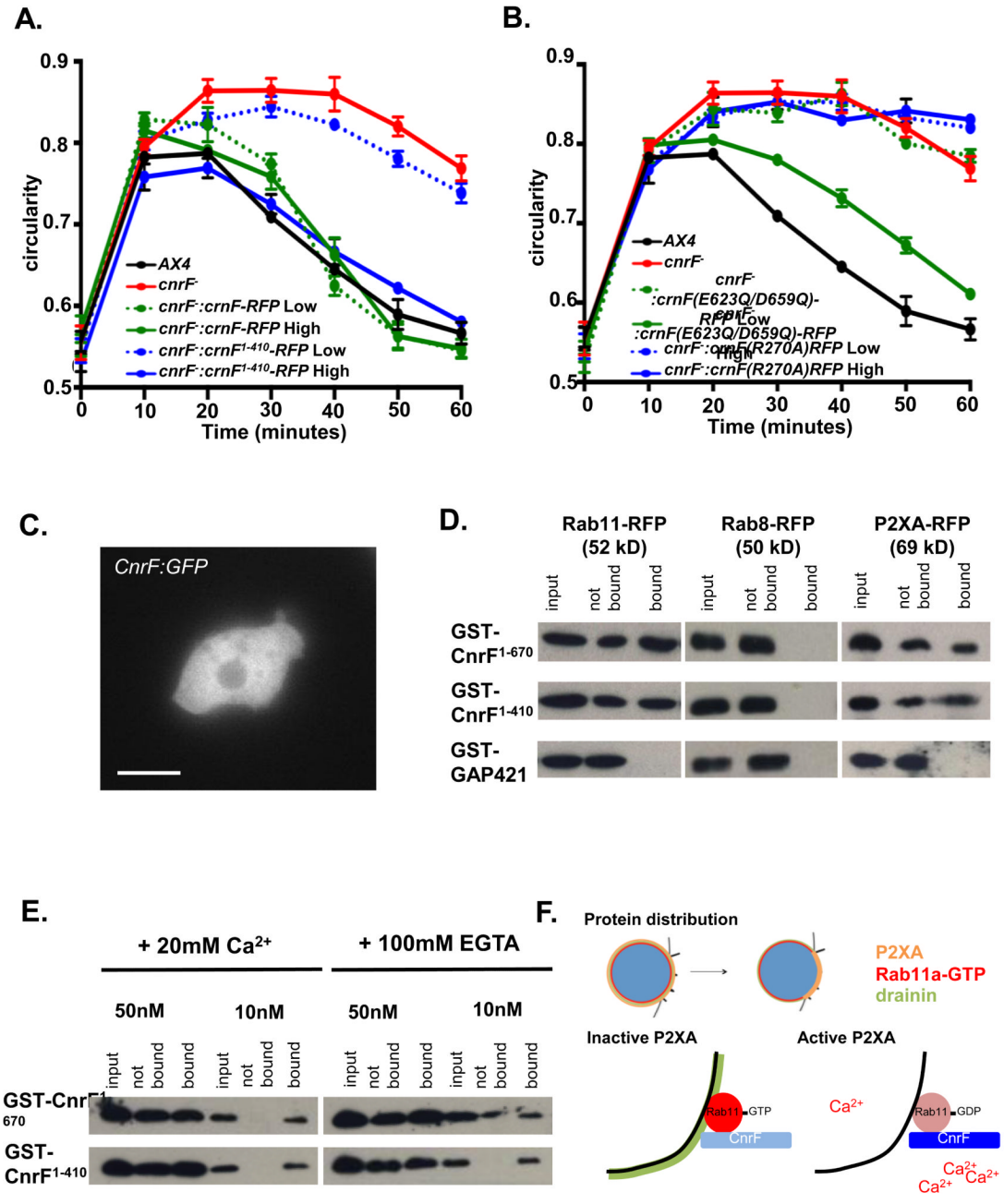

Figure 8. cnrF is a cytosolic calcium dependent Rab11a GAP that interacts with P2XA and Rab11a

A. Rescue of *cnrF* mutant null phenotype by full-length (1-670) *cnrF-RFP* and a truncated (1-410) form of *cnrF-RFP* that lacks the EF hands. Cell lines were selected based on RFP expression levels. Both *CnrF*$^{-}$ *CnrF*$^{1\text{-}670}$ *Low* (2064 A.U.), *CnrFCnrF*$^{1\text{-}670}$ *High* (10106 A.U.) and *CnrF*$^{-}$ *CnrF*$^{1\text{-}410}$ *High* (9987 A.U.) cells show an indistinguishable hypoosmotic shock response to wild type (Paired T test p>0.01). However, *CnrF*$^{-}$ *CnrF*$^{1\text{-}410}$ *Low* (2111 A.U.) cells fail to rescue the mutant phenotype (Paired T test p>0.05). Error bars represent s.e.m. and results are means of n=3 independent experiments, each with 100 cells. Statistical source data for Fig 8A can be found in Supplementary Table 2.B. Rescue of *cnrF*$^{-}$ mutant

Europe PMC Funders Author Manuscripts

phenotype by a point mutated forms of *cnrF-RFP* that disrupt the EF hands (cnrF(E623Q/D659Q)) or rab GAP activity (cnrF(R270A)). *CnrF(*E623Q/D659Q*)-RFP* low cells (2044 a.u.) fail to rescue the mutant phenotype (Paired T test $p>0.05$), whereas cells expressing high levels of *CnrF(*E623Q/D659Q*)-RFP* (9946 A.U.) show a similar hypoosmotic shock response to wild type (Paired T test $p>0.05$). Both low levels of *CnrF*(R270*)-RFP* expression (1998 A.U.) and high levels of *CnrF*(R270*)-RFP* expression (10042 A.U.) fail to rescue the mutant phenotype (Paired T test $p>0.05$). Error bars represent s.e.m. and results are means of n=3 independent experiments, each with 100 cells. Statistical source data for Fig 8B can be found in Supplementary Table 2. C. *CnrF:GFP* expression in wild type cells. Scale bar = 5 μm. D. Rab11a and P2XA (but not Rab8a) bind GST-CnrF$^{1-670}$ or GST-CnrF$^{1-410}$, but not GST-RabGAP421 control (a related *Dictyostelium* EF hand domain containing RabGAP (DDB_G0275421)). E. Rab11a binding to CnrF is not calcium dependent. Varying amounts of protein from cells expressing Rab11a:RFP were incubated with beads bound with GST-CnrF$^{1-670}$ or GST-CnrF$^{1-410}$ in 20mM Ca^{2+} or 100mM EGTA. F. Proposed model of P2XA regulated vesicle fusion. Maturing vacuoles expresses P2XA, Rab11a-GTP and Drainin. Once tethered, P2XA undergoes a ‘ring to patch’ transition so that P2XA is only expressed at the plasma membrane contact site. Concentration of P2XA activity leads to a localized increase in calcium ions as they pass through the active channel. Consequently, P2XA bound CnrF is activated as Ca^{2+} binds to the EF hand domain on CnrF, leading to the hydrolysis and inactivation of Rab11a-GTP, and therefore inactivation of Drainin at the plasma membrane contact site.